Science of the Total Environment 612 (2018) 1141–1148

Contents lists available at ScienceDirect

Science of the Total Environment

journal homepage: www.elsevier.com/locate/scitotenv

Spatiotemporal evolution of the chlorophyll *a* trend in the North Atlantic Ocean

Min Zhang [a,b,c], Yuanling Zhang [a,b,c], Qi Shu [a,b,c], Chang Zhao [a,b,c], Gang Wang [a,b,c], Zhaohua Wu [c,d], Fangli Qiao [a,b,c,*]

[a] First Institute of Oceanography, State Oceanic Administration, Qingdao, China
[b] Laboratory for Regional Oceanography and Numerical Modeling, Qingdao National Laboratory for Marine Science and Technology, Qingdao, China
[c] Key Laboratory of Data Analysis and Applications, State Oceanic Administration, Qingdao, China
[d] Department of Earth, Ocean, and Atmospheric Science, Center for Ocean-Atmospheric Prediction Studies, Florida State University, Tallahassee, USA

HIGHLIGHTS

- Spatiotemporal evolution of chlorophyll *a* trend in the North Atlantic Ocean was firstly obtained.
- The time-varying trend of chlorophyll *a* shows a dipole pattern and a propagation signal.
- The pattern of the chlorophyll *a* trend during the recent two decades is a part of the multidecadal variation.
- These patterns of chlorophyll *a* trend are possibly regulated by the changes of Atlantic Meridional Overturning Circulation.

GRAPHICAL ABSTRACT

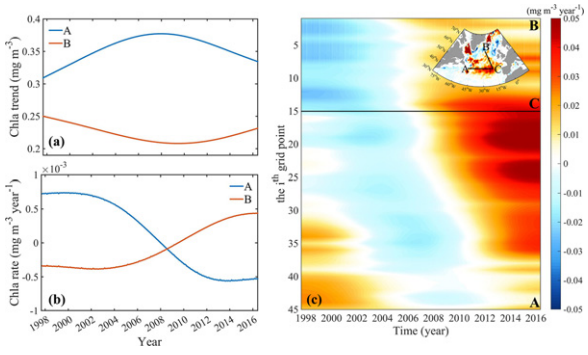

ARTICLE INFO

Article history:
Received 10 August 2017
Received in revised form 29 August 2017
Accepted 30 August 2017
Available online 8 September 2017

Editor: D. Barcelo

Keywords:
Chlorophyll *a*
Spatiotemporal evolution
The variable trend
Dipole pattern
Propagation
Multidimensional ensemble empirical mode decomposition

ABSTRACT

Analyses of the chlorophyll *a* concentration (chla) from satellite ocean color products have suggested the decadal-scale variability of chla linked to the climate change. The decadal-scale variability in chla is both spatially and temporally non-uniform. We need to understand the spatiotemporal evolution of chla in decadal or multidecadal timescales to better evaluate its linkage to climate variability. Here, the spatiotemporal evolution of the chla trend in the North Atlantic Ocean for the period 1997–2016 is analyzed using the multidimensional ensemble empirical mode decomposition method. We find that this variable trend signal of chla shows a dipole pattern between the subpolar gyre and along the Gulf Stream path, and propagation along the opposite direction of the North Atlantic Current. This propagation signal has an overlapping variability of approximately twenty years. Our findings suggest that the spatiotemporal evolution of chla during the two most recent decades is part of the multidecadal variations and possibly regulated by the changes of Atlantic Meridional Overturning Circulation, whereas the mechanisms of such evolution patterns still need to be explored.

1. Introduction

Marine phytoplankton is responsible for nearly half of the global primary production (Behrenfeld et al., 2001). Long-term changes in marine

* Corresponding author at: First Institute of Oceanography, State Oceanic Administration, Qingdao, China.
E-mail address: qiaofl@fio.org.cn (F. Qiao).

http://dx.doi.org/10.1016/j.scitotenv.2017.08.303
0048-9697/

phytoplankton could have potentially significant effects on the ocean food web and the global biogeochemical cycle. Detecting the trend of phytoplankton and the impact of physical processes on the phytoplankton trend are an essential task (Henson et al., 2010). The satellite-observed ocean chlorophyll *a* concentration (hereafter, chla) is the most commonly used index of the phytoplankton biomass and thus of phytoplankton changes (McClain, 2009). Over two decades of ocean color sensor records have provided us a chance to examine the relatively long-term changes/trends in both the spatial and temporal distributions of chla from space (Maritorena et al., 2010).

Traditional linear regression analysis has been widely used to assess the trend of chla (Gregg et al., 2005; Behrenfeld et al., 2006; Martinez et al., 2009; Yoder et al., 2010; Henson et al., 2010; Boyce et al., 2010; Rousseaux and Gregg, 2015). However, this most commonly used linear best fitted trend requires longer data records, and changes with different temporal or spatial scales (Henson et al., 2010; Palacz et al., 2011), which make it difficult to reveal the true long-term trend of chla. Because the long-term changes in chla are spatially and temporally non-uniform, we need to understand the evolution of chla both spatially and temporally to better evaluate the impact of the physical variations on ecosystem structures and the potential biogeochemical effect of long-term changes in phytoplankton on decadal and longer timescales.

Spatiotemporal changes in phytoplankton are mainly controlled by variations of biological sources and physical forcings (Behrenfeld et al., 2006; Charria et al., 2006; Olonscheck et al., 2013), both of which have been shown to be sensitive to climate change (Gregg et al., 2005; Boyce et al., 2010). The response of marine phytoplankton to the various physical processes has likely occurred over long timescales (Antoine et al., 2005), with the declining trend related to the increasing sea surface temperature (Gregg et al., 2005; Boyce et al., 2010), changes in wind and buoyancy forcing (Lozier et al., 2011), and the reduction in the Atlantic Meridional Overturning Circulation (AMOC) (Schmittner, 2005). Model simulations suggest that changes in the AMOC are significantly correlated with the decadal variations in chla and nutrient concentrations (Sanchez-Franks and Zhang, 2015). Although a declining trend in chla may have occurred, chla trends from different sets of measurements may lead to large biases and uncertainties (Mackas, 2011). To distinguish a global warming trend from natural variability, Henson et al. (2010) pointed out that continuous data lengths of at least 40-year are needed. However, the longest available continuous observational dataset for chla spans just over two decades (Maritorena et al., 2010). Therefore, new analytical methods are urgently needed to gain deeper insights into this two-decade long chla dataset. Moreover, studies based on observational datasets have yet to show how the spatiotemporal evolution of chla responds to the variations in biological sources and physical forcings.

This study focuses on how the chla trend in the North Atlantic Ocean has evolved based on the available longest merged ocean color records from 1997 to 2016. We extract the variable trend of chla using the multi-dimensional ensemble empirical mode decomposition method, and then examine the spatiotemporal evolution pattern of chla in the North Atlantic Ocean. Moreover, the potential linkage between spatiotemporal evolution patterns of chla and the changes of AMOC is also discussed.

2. Data and methods

2.1. Data

Merged satellite ocean color products obtained from multiple sensors (SeaWiFS, MERIS, MODIS-Aqua, VIIRS) from 1997 to 2016 were provided by the European Space Agency GlobColour project (http://www.globcolour.info/). This merged product not only extends the data lengths but also significantly improves the spatial and temporal

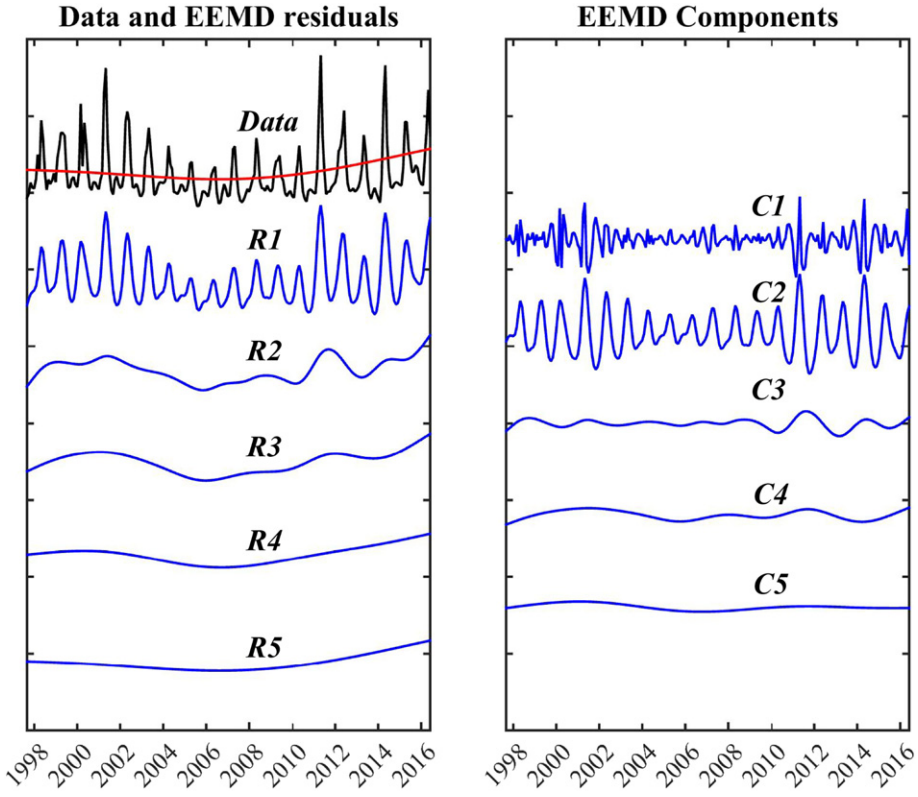

Fig. 1. EEMD decomposition of the averaged chla in the North Atlantic (40–48°N, 15–30°W). In the left panel, the original data (black) and successive remainders (R_j: R_1 to R_5 in this case) after an additional EEMD component (C_j: C_1 to C_5 in this case) are extracted, i.e., $R_j = R_{j-1} - C_j$ for $j > 1$. The red line is the EEMD trend R_n (R_5 in this case). In the right panel, each line represents an EEMD component (C_j) from high frequency to low frequency.

coverage and lowers uncertainties (Maritorena and Siegel, 2005; Maritorena et al., 2010). Here, we choose the monthly chla products generated from a weighted averaging technique with approximately 100 km spatial resolution, which shows the significant gain in coverage. We focus only on the deep basin water, and data of shelf waters (<200 m depth) are not considered.

We also analyze the time-varying trend of the observational-based AMOC time series at both 26.5°N and 41°N. The AMOC time series at 26.5°N are from the RAPID/MOCHA array across the Atlantic Ocean (http://www.rapid.ac.uk/rapidmoc) (Kanzow et al., 2007; McCarthy et al., 2012, 2015; Srokosz and Bryden, 2015). The AMOC estimate at 41°N from January 2002 to September 2010 are from Willis (2010), which was derived using a combination of Argo floats and satellite altimeter data.

2.2. Methods

To extract and diagnose the spatiotemporally varying trend of the chla, we use the multidimensional ensemble empirical mode decomposition (MEEMD) method (Wu et al., 2009), which is based on ensemble empirical mode decomposition (EEMD) (Wu and Huang, 2009) and empirical mode decomposition (EMD) (Wu and Huang, 2004; Huang et al., 1998). EMD, EEMD and MEEMD have been widely applied to ocean and climate research (Huang and Wu, 2008; Ji et al., 2014; Franzke, 2014; Chen et al., 2017).

In MEEMD, the chla time series at any spatial location is firstly decomposed into a series of amplitude-frequency modulated oscillatory components C_j ($j = 1, 2, \ldots, n$) and a residual trend R_n from high-frequency to low-frequency using EEMD (Figs. 1 and S1).

$$x(t) = \sum_{j=1}^{n} C_j(t) + R_n(t)$$

R_n is the time-varying trend, which is an intrinsically fitted monotonic function or a function with at most one extremum. This residue trend R_n varies with time after adaptively removing all the oscillatory components, which require no a priori functional form. As the reality

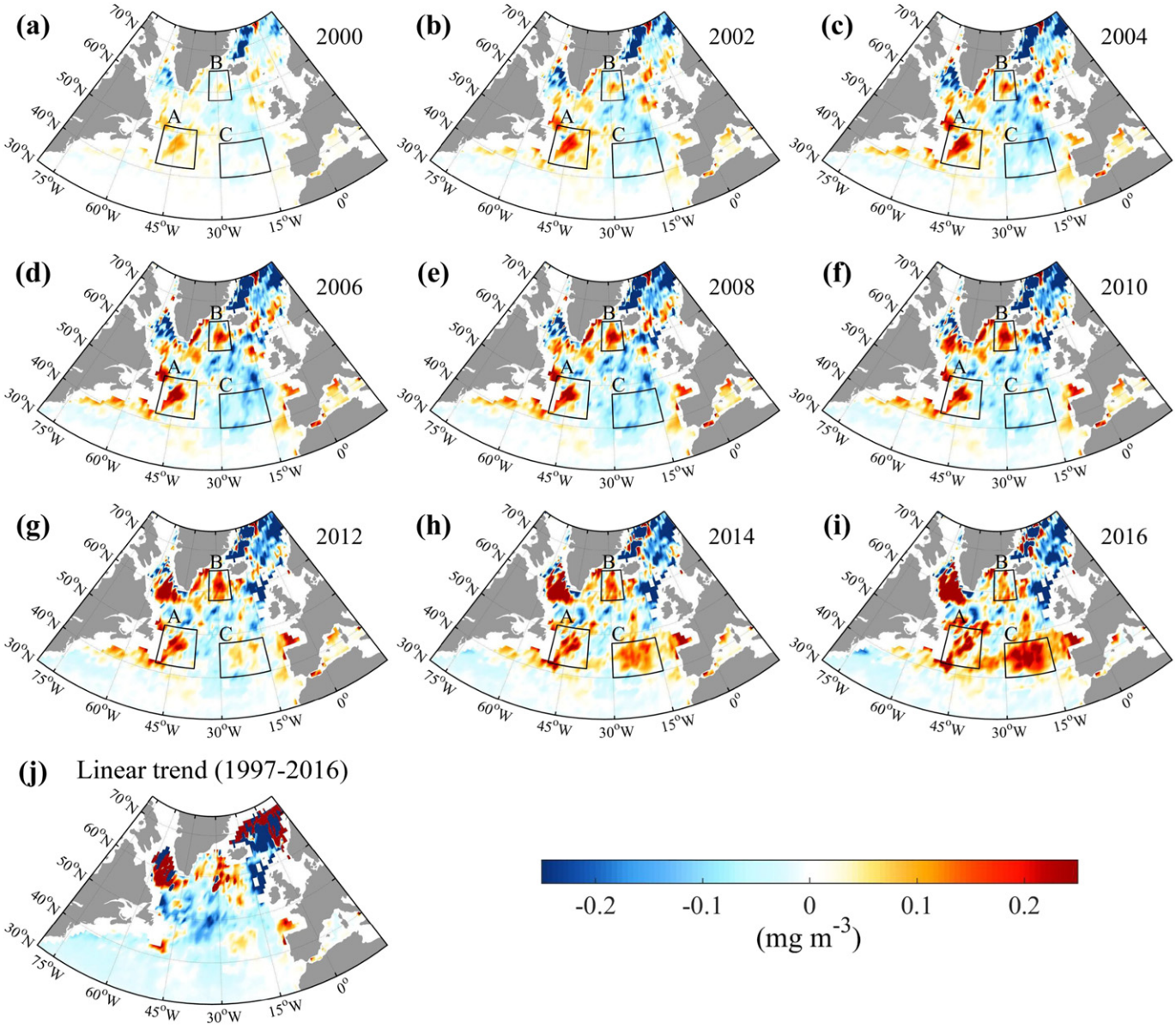

Fig. 2. Spatiotemporal evolution of the MEEMD trends of ocean surface chla in the North Atlantic Ocean. a–i, MEEMD trends (mg m^{-3}) ending in 2000, 2002, 2004, 2006, 2008, 2010, 2012, 2014 and 2016, respectively. j, Spatial structure of chla increase based on the time-unvarying linear trend over the entire data domain from 1997 to 2016. A, B, and C indicated by black boxes refer to the North Gulf Stream region, the subpolar gyre region, and the region near the West European basin and Iberian basin, respectively.

that has already happened cannot be changed by the subsequent system, this adaptively time-varying trend has low sensitivity to the extension of new data (Fig. S2). For multidimensional chla dataset, we then piece together all the corresponding components (C_j or R_n) of all the time series from all spatial locations to obtain the temporal evolution of the spatially coherent features of that timescale (Figs. S3, S4 and Supplementary information for more details). Compared with the traditional empirical orthogonal function analysis, the MEEMD result could present both the spatial and temporal local information due to its adaptiveness and locality (Figs. S2–S4), which has the capability to reflect the hidden nonlinear and nonstationary nature of a time series (Wu et al., 2007; Wu et al., 2011; Ji et al., 2014; Franzke, 2014). Detailed information can be found in Wu et al. (2009) and supplementary information.

To examine the spatiotemporal evolution of the chla trend on decadal timescales or longer, we only focus on the residue trend R_n after adaptively removing all of the C_j contained in the chla time series. Due to the time-varying nature of the MEEMD trend and to facilitate the comparison with the traditional linear trend, we follow Ji et al. (2014) to define the chla increment at a particular temporal location t as the increment of the $R_n(t)$ with respect to its trend value from the reference time at 1998 ($R_n(1998)$), i.e., $R_n(t) - R_n(1998)$.

3. Results and discussion

3.1. Spatiotemporal evolution of the chla trend and rate

The spatial evolution of chla increments by a given time is presented in Fig. 2 (Movie S1). A noticeable initial increasing signal of chla (>0.1 mg m^{-3}) first appears in the North Gulf Stream (region A, 42°–51°N, 38°–50°W) in 2000, when there are few signs of chla increasing (<0.05 mg m^{-3}) elsewhere in the North Atlantic region. The chla in the subpolar gyre region (region B, 58°–65°N, 24°–34°W) starts to show an increasing signal two years later. The chla increment in most of regions A and B reach their maximum (>0.2 mg m^{-3}) in 2006 and 2010, respectively. After 2010, the chla increasing signal (>0.05 mg m^{-3}) starts to expand southward into the region near the

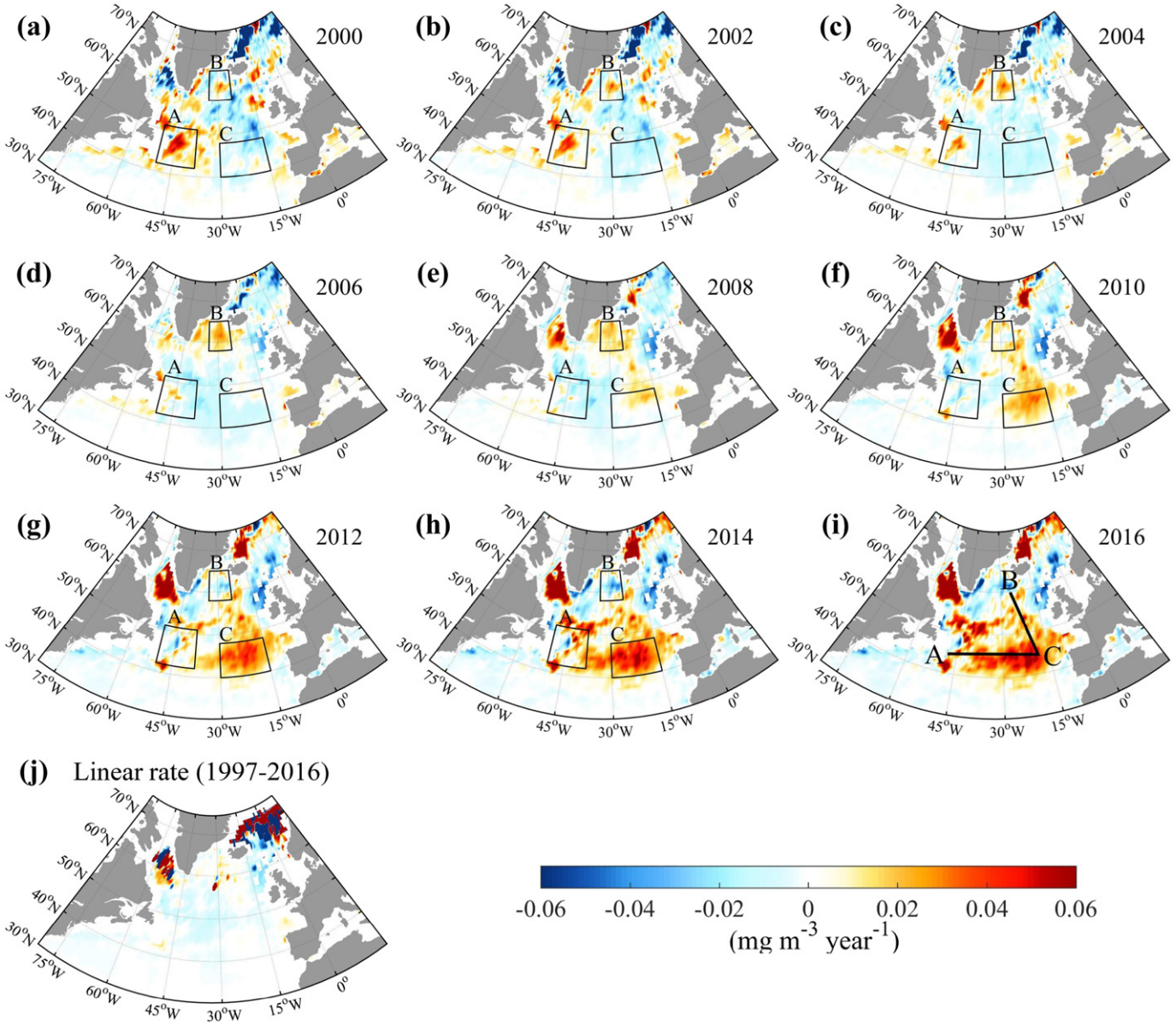

Fig. 3. The instantaneous rate of the chla trend in the North Atlantic Ocean. a–i, Instantaneous rate of the chla trend (mg m^{-3} $year^{-1}$) in 2000, 2002, 2004, 2006, 2008, 2010, 2012, 2014 and 2016, respectively. j, Spatial structure of the instantaneous rate based on the time-unvarying linear trend over the entire data domain from 1997 to 2016. i, Black line depicts the propagation path of the chla increasing signal from region B to C and back to A.

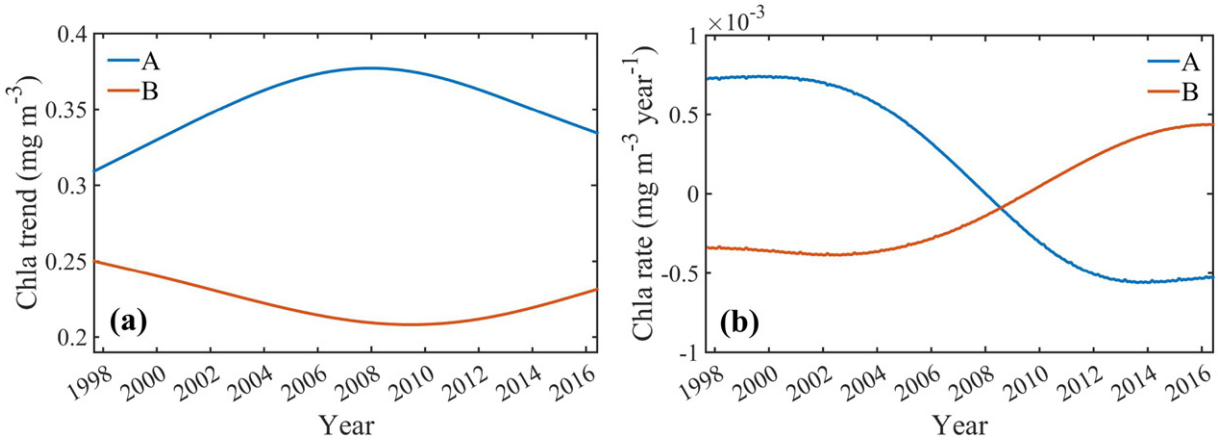

Fig. 4. The dipole pattern of regional averaged chla trend (a) and rate (b) for the north Gulf Stream region (A) and the subpolar gyre region (B).

West European basin and Iberian basin (region C, 40°–48°N, 15°–30°W) and accumulates in this region, which then expands westward back to region A. Based on the spatiotemporal evolution pattern of the chla increment, it appears that the chla increasing signal starts in region A, and then region B, with a propagating process from region B to region C and back to region A. This clockwise low-frequency evolution and propagation of chla cannot be revealed by the linear trend over the same period (Fig. 2j).

Owing to the time-varying nature of the chla trend shown above, the corresponding instantaneous rates are also spatially and temporally variable, which can be determined by calculating the temporal derivatives of the chla trend. The instantaneous increasing/decreasing rate of the chla trend is shown in Fig. 3 (Movie S2). The increasing rate in region A began in 1998 and shrank from 1998 to 2006, then turned into decreasing region from 2006 to 2010 and back to show increasing signal from 2012 (Movie S2). In contrast, the increasing rate in region B enlarged until 2008 and then turned into decreasing rate in most part of the region after 2012. After 2006, a clear propagation signal of the chla increasing rate can be observed from region B to region C and then back to region A. It is noted that the spatial structure of the increasing/decreasing rate of the chla trend over the whole temporal domain cannot be determined from straight line fitting (Fig. 3j).

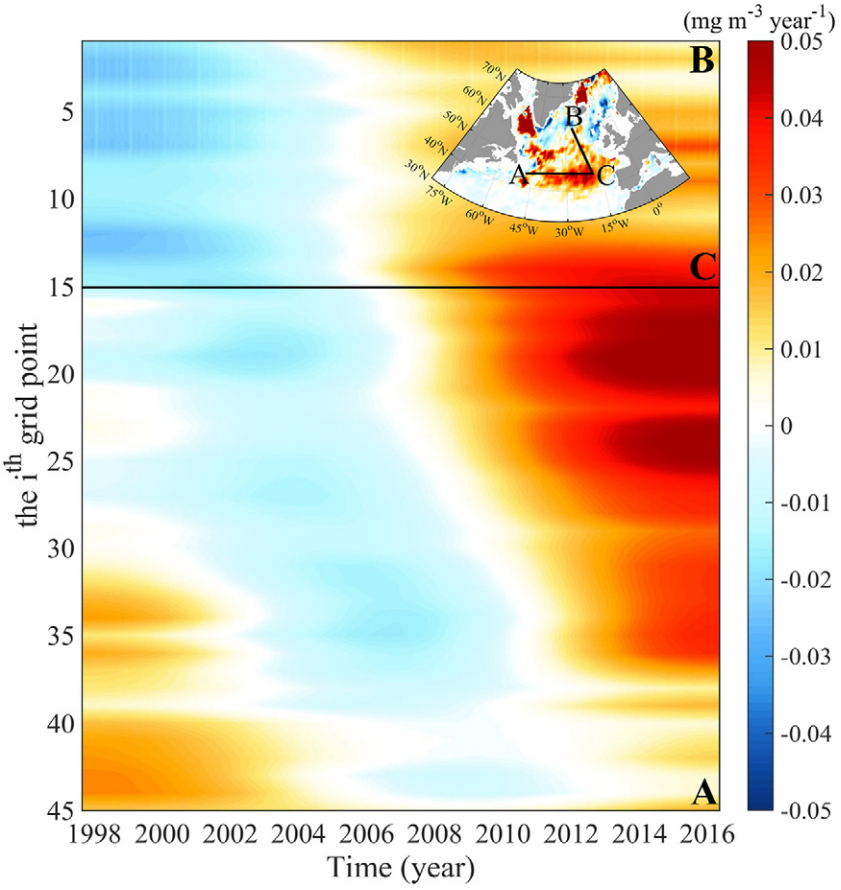

Fig. 5. Hovmöller diagrams of the rate of surface chla. In total, 45 grid points are selected: the y axis denotes the ith ($i = 1, 2, \ldots, 45$) grid point following the path from the subpolar gyre region (B) to the region near the west European basin and Iberian basin (C), and back to the north Gulf Stream region (A) shown in the embedded panel, with the colorbar indicating the value of the chla rate (mg m^{-3} $year^{-1}$).

Two noticeable patterns can be discerned from the spatiotemporal evolution of the chla trend and rate: (1) the noticeable time lag of the chla increasing signal between region A and region B, and (2) the propagation of the chla increasing signal from region B to region C and back to region A.

3.2. Chla dipole patterns and propagation

As shown in Figs. 2 and 3, there is a time lag of the chla increasing signal between region A and region B. When the chla in region A increases, the chla in region B shows a decreasing pattern, and vice-versa. Thus, the averaged time-varying trend and corresponding instantaneous changing rates of chla in region A and B are used to compare the evolution patterns between these two regions (Fig. 4). Before 2008, the chla in region A increases with a slowing increasing rate, whereas, the chla in region B shows a decreasing pattern with a slowing decreasing rate. After 2008, the chla in region A shows a decreasing pattern with the rate of decrease slowing down, whereas the chla in region B increases with the rate of increase speeding up. This dipole pattern of the chla trend/rate evolution also appears in satellite sea surface temperature (SST, Fig. S5) and sea surface height (SSH, Fig. S6). Due to the lack of continuous ocean color observations before 1997, it remains to be clarified whether this dipole pattern in regions A and B is a decadal variation or a long-term trend. However, the time-varying trend and rate of chla extracted from MEEMD in this study have low sensitivity to the addition of new data (Fig. S2).

The other intriguing pattern is that the increasing rate of chla propagates clockwise from region B to region C and back to region A. Hovmöller diagrams of this time-varying rate of the chla clearly reveal this propagation process (Fig. 5), with the temporal axis covering the period from 1997 to 2016. The chla increasing signal in region B starts to propagate around 2004, and extends rapidly to region C in two to three years, and then further extends to region A in the following ten years. In addition to this propagation of the chla increasing signal, we also find that the chla decreasing signal propagates along the same route from the years before 1997 to 2010. This flipped contrast between the increasing and decreasing signals of chla trends implies that this increasing and decreasing oscillation has a period of about twenty years. This oscillation could be an internal multi-decadal variation that is probably correlated with the changes of ocean circulation or the variations of the physical forcings.

3.3. Mechanisms discussion

The dipole pattern and the clockwise propagation of the chla trend in decadal/multidecadal timescales in the North Atlantic Ocean shown above could possible link to the variations in the strength of the subpolar gyre, the North Gulf Stream, and the North Atlantic Current. These variations in the strength of the circulation are linked to the changes in the AMOC (Sanchez-Franks and Zhang, 2015), as well as changes in ocean physical and biological parameters.

In this study, we have tested all the possible physical and biological variables (Talley et al., 2011), including sea surface temperature (SST), wind stress/curl, sea surface height (SSH), photosynthetic available radiation, aerosol optical depth (Figs. S5 and S6 for example), it is hard to explain why the ocean surface chla trend has evolved as shown in Figs. 2 and 3 (Movies S1 and S2). Zhang (2008) has suggested that the dipole pattern between the subpolar gyre and the Gulf Stream path in terms of the SSH and subsurface temperature is a distinctive fingerprint of the AMOC variability. Häkkinen and Rhines (2004) also concluded that the observed SSH trend during the 1990s indicates a weakening of the subpolar gyre. Thus the dipole pattern of chla/SST/SSH trends between the subpolar gyre and the Gulf Stream path (Figs. S8 and S9) in this study may be tied to the changes in the AMOC. We further diagnose the time series of the overturning transports (MOC) at 26.5°N and 41°N (Willis, 2010; Srokosz and Bryden, 2015; Lozier et al., 2017). The time-varying trends of the MOC extracted from the time series at 26.5°N and 41°N both show clearly declining trends, starting from 2004 and 2005, respectively (Fig. 6). The weakening MOC has been shown to be revealed by the dipole pattern of the SSH between the subpolar gyre and the North Gulf Stream path region (Zhang, 2008; Figs. S5 and S6). This weakening MOC and the dipole pattern of the SSH/SST may further regulate the chla distribution on inter-annual, decadal, or even longer time scales. The chla shows positive response to the SST in the dipole region (Figs. 3, S5, 7). This positive relationship has been observed in the Northeast Atlantic Ocean north of 50°N (Richardson and Schoeman, 2004), with the increasing water temperature normally leading to increased phytoplankton metabolic rates and stronger stratification, and thus increased phytoplankton abundance (Fig. 7).

The other prominent characteristic of the spatiotemporal evolution of chla is the obvious clockwise propagation signal from region B to C and then to A (Fig. 3i). This propagation route coincides with one branch of the North Atlantic Current (NAC) based on the upper ocean current reanalysis results from ECMWF Ocean reanalysis System 4 (Balmaseda et al., 2013; Fig. S8), but in the opposite direction. Further investigation of the spatiotemporal evolution of the upper ocean current trend shows decreasing signal along the partial route of the NAC (Fig. S7). On the basis of the decreasing trend of the MOC at 41°N after 2006 (Fig. 6b), we speculate that the NAC is also weakened by the weakening of the MOC during the recent decade (Fig. S9). The chla propagation from region B to C and then to A, in the opposite direction of the NAC, could possibly regulated by the horizontal advection of the chla gradients accompanied by the weakening of the NAC (Charria et al., 2006). To confirm this assumption, we average the chla in region C near the West European basin and Iberian basin (40°–48°N, 15°–30°W) to check whether the time-varying trend of chla is consistent with the AMOC changes at 41°N. The time-varying trend of chla in this region coincides

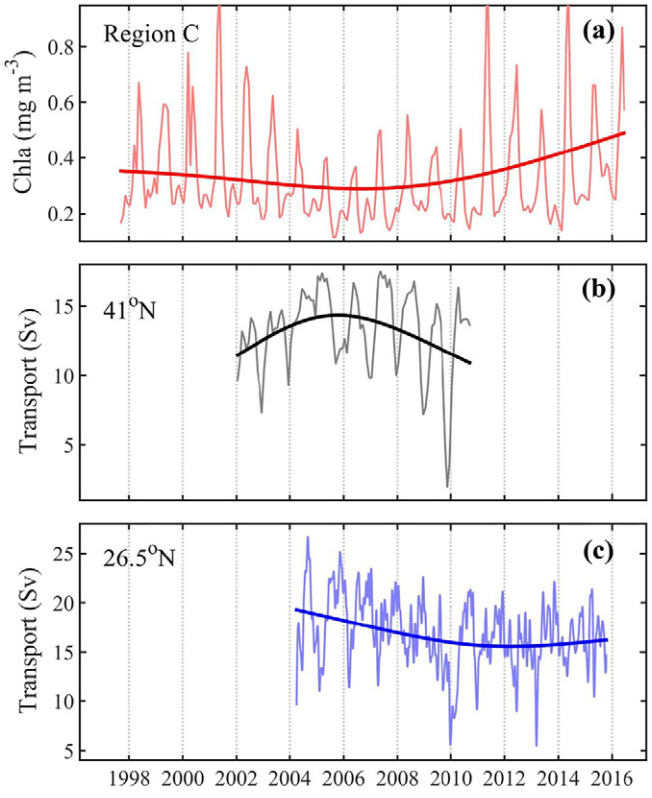

Fig. 6. Time series and the time-varying trend of chla and MOC. a, Monthly chla time series and the time-varying trend in region C near the West European basin and Iberian basin (40°–48°N, 15°–30°W); b, MOC time series at 41°N for the period January 2002 to September 2010 from Willis (2010) and its time-varying trend; and c, MOC time series at 26.5°N for the period April 2004 to October 2015 and its time-varying trend. The light curves and heavy curves represent the time series and the time-varying trend, respectively.

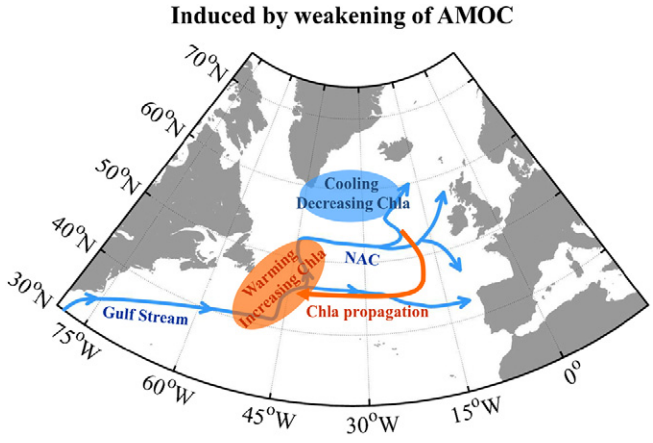

Fig. 7. Schematic diagram of the possible links between chla evolution patterns and the weakening of the AMOC. The route of the North Atlantic Current is referred from Talley et al. (2011) and Lozier et al. (2017). Blue indicates a decreasing or weakening trend, whereas orange indicates an increasing trend or propagation.

with the AMOC changes at 41°N but in the opposite direction (Fig. 6), both having a turning point in 2006, which implying that the changes in the AMOC may have played a role in regulating the spatiotemporal evolution of the chla in decadal/multidecadal timescales (Fig. 7).

It is noted that the mechanism discussion above contains large uncertainties because we are unable to provide more evidence to the linkage between the chla patterns and the changes of AMOC, as well as the changes of the NAC. Moreover, the roles of the AMOC and the NAC in modulating the spatiotemporal evolution of the chla on decadal/multidecadal timescales require further investigation when the ongoing observations from ocean color satellite and subsurface temperature measurements (such as the ARGO program) become available and more abundant in the future decades.

4. Conclusions

The almost two-decade data of the global ocean chla from merged ocean color products may be insufficient to characterize the long-term trends on multi-decadal or even longer time scales. However, these time series are sufficiently long to examine the relatively long-term trend. Moreover, the time-varying trend of chla extracted with MEEMD method would not change with the extension of new data. Thus, the results of this study are intended to serve as a benchmark for studying the decadal and multi-decadal variability in marine ecosystem.

This study focuses on the open ocean in the North Atlantic, which is characterized by high primary productivity. Based on MEEMD, we examine the chla trends from a new perspective. The time-varying trend of chla reveals a dipole pattern between the regions in the subpolar gyre and the North Gulf Stream path, and propagation in the opposite direction of the NAC. Our findings suggest that the spatiotemporal evolution of chla during the two most recent decades is part of the multidecadal variations and could possibly be due to the changes of Atlantic Meridional Overturning Circulation, whereas the explanations for why the surface chla trend in the North Atlantic Ocean has evolved still need to be explored.

Supplementary data to this article can be found online at http://dx.doi.org/10.1016/j.scitotenv.2017.08.303.

Acknowledgments

We thank the ESA GlobColour project (http://www.globcolour.info/) for providing the merged satellite L3 ocean color product. Data from the RAPID-WATCH MOC monitoring project funded by the Natural Environment Research Council are freely available at http://www.rapid.ac.uk/rapidmoc/. A MATLAB code package for the EEMD method is freely downloadable at http://rcada.ncu.edu.tw/research1.htm. M. Zhang and Y. Zhang were jointly supported by the National Natural Science Foundation of China under Grant 41206027, the Basic Scientific Fund for National Public Research Institutes of China under Grants 2013G20 and 2012G23, and the National Programme on Global Change and Air-Sea Interaction under Grant GASI-03-01-02-01. F. Qiao, Q. Shu, C. Zhao, and G. Wang were jointly supported by the International cooperation project on the China-Australia Research Centre for Maritime Engineering of Ministry of Science and Technology, P. R. China under Grant 2016YFE0101400, NSFC-Shandong Joint Fund for Marine Science Research Centers under Grant U1406404, the National Programme on Global Change and Air-Sea Interaction under Grant GASI-IPOVAI-05, and the AoShan Talents Program supported by Qingdao National Laboratory for Marine Science and Technology under Grant 2015ASTP.

References

Antoine, D., Morel, A., Gordon, H.R., Banzon, V.F., Evans, R.H., 2005. Bridging ocean color observations of the 1980s and 2000s in search of long-term trends. J. Geophys. Res. 110:C06009. http://dx.doi.org/10.1029/2004JC002620.

Balmaseda, M.A., Mogensen, K., Weaver, A., 2013. Evaluation of the ECMWF ocean reanalysis ORAS4. Q. J. R. Meteorol. Soc. 139:1132–1161. http://dx.doi.org/10.1002/qj.2063.

Behrenfeld, M.J., Randerson, J.T., McClain, C.R., Feldman, G.C., Los, S.O., Tucker, C.J., Falkowski, P.G., Field, C.B., Frouin, R., Esaias, W.E., Kolber, D.D., Pollack, N.H., 2001. Biospheric primary production during an ENSO transition. Science 291 (5513): 2594–2597. http://dx.doi.org/10.1126/science.1055071.

Behrenfeld, M.J., O'Malley, R.T., Siegel, D.A., McClain, C.R., Sarmiento, J.L., Feldman, G.C., Milligan, A.J., Falkowski, P.G., Letelier, R.M., Boss, E.S., 2006. Climate-driven trends in contemporary ocean productivity. Nature 444:752–755. http://dx.doi.org/10.1038/nature05317.

Boyce, D.G., Lewis, M.R., Worm, B., 2010. Global phytoplankton decline over the past century. Nature 466:591–596. http://dx.doi.org/10.1038/nature09268.

Charria, G., Dadou, I., Cipollini, P., Drévillon, M., De Mey, P., Garçon, V., 2006. Understanding the influence of Rossby waves on surface chlorophyll concentrations in the North Atlantic Ocean. J. Mar. Res. 64:43–71. http://dx.doi.org/10.1357/002224006776412340.

Chen, X.Y., Zhang, X.B., Church, J.A., Watson, C.S., King, M.A., Monselesan, D., Legresy, B., Harig, C., 2017. The increasing rate of global mean sea-level rise during 1993–2014. Nat. Clim. Chang. 7:492–495. http://dx.doi.org/10.1038/NCLIMATE3325.

Franzke, C.L.E., 2014. Warming trends: nonlinear climate change. Nat. Clim. Chang. 4: 423–424. http://dx.doi.org/10.1038/NCLIMATE 2245.

Gregg, W.W., Casey, N.W., McClain, C.R., 2005. Recent trends in global ocean chlorophyll. Geophys. Res. Lett. 32:L03606. http://dx.doi.org/10.1029/2004GL021808.

Häkkinen, S., Rhines, P.B., 2004. Decline of subpolar North Atlantic circulation during the 1990s. Science 304 (5670):555–559. http://dx.doi.org/10.1126/science.1094917.

Henson, S.A., Sarmiento, J.L., Dunne, J.P., Bopp, L., Lima, I., Doney, S.C., John, J., Beaulieu, C., 2010. Detection of anthropogenic climate change in satellite records of ocean chlorophyll and productivity. Biogeosciences 7, 621–640.

Huang, N.E., Wu, Z., 2008. A review on Hilbert-Huang transform: method and its applications on geophysical studies. Rev. Geophys. 46:RG2006. http://dx.doi.org/10.1029/2007RG000228.

Huang, N.E., Shen, Z., Long, S.R., Wu, M.C., Shin, H.H., Zheng, Q., Yen, N.C., Tung, C.C., Liu, H.H., 1998. The empirical mode decomposition and the Hilbert spectrum for nonlinear and non-stationary time series analysis. Proc. R. Soc. Lond. A 454:903–995. http://dx.doi.org/10.1098/rspa.1998.0193.

Ji, F., Wu, Z., Huang, J., Chassignet, E.P., 2014. Evolution of land surface air temperature trend. Nat. Clim. Chang. 4:462–466. http://dx.doi.org/10.1038/NCLIMATE2223.

Kanzow, T., Cunningham, S.A., Rayner, D., Hirschi, J.J.-M., Johns, W.E., Baringer, M.O., Bryden, H.L., Beal, L.M., Meinen, C.S., Marotzke, J., 2007. Observed flow compensation associated with the MOC at 26.5°N in the Atlantic. Science 317 (5840):938–941. http://dx.doi.org/10.1126/science.1141293.

Lozier, M.S., Dave, A.C., Palter, J.B., Gerber, L.M., Barber, R.T., 2011. On the relationship between stratification and primary productivity in the North Atlantic. Geophys. Res. Lett. 38 (18):L8609. http://dx.doi.org/10.1029/2011GL049414.

Lozier, M., Bacon, S., Bower, A., et al., 2017. Overturning in the Subpolar North Atlantic Program: a new international ocean observing system. Bull. Am. Meteorol. Soc. 98: 737–752. http://dx.doi.org/10.1175/BAMS-D-16-0057.1.

Mackas, D.L., 2011. Does blending of chlorophyll data bias temporal trend? Nature 472: E4–E5. http://dx.doi.org/10.1038/nature09951.

Maritorena, S., Siegel, D.A., 2005. Consistent merging of satellite ocean color data sets using a bio-optical model. Remote Sens. Environ. 94:429–440. http://dx.doi.org/10.1016/j.rse.2004.08.014.

Maritorena, S., d'Andon, O.H.F., Mangin, A., Siegel, D.A., 2010. Merged satellite ocean color data products using a bio-optical model: characteristics, benefits and issues. Remote Sens. Environ. 114:1791–1804. http://dx.doi.org/10.1016/j.rse.2010.04.002.

Martinez, E., Antoine, D., D'Ortenzio, F., Gentilti, B., 2009. Climate-driven basin-scale decadal oscillations of oceanic phytoplankton. Science 326:1253–1256. http://dx.doi.org/10.1126/science.1177012.

McCarthy, G., Frajka-Willams, E., Johns, W.E., Baringer, M.O., Meinen, C.S., Bryden, H.L., Rayner, D., Duchez, A., Roberts, C., Cunningham, S.A., 2012. Observed interannual

variability of the Atlantic meridional overturning circulation at 26.5°N. Geophys. Res. Lett. 39:L19609. http://dx.doi.org/10.1029/2012GL052933.
McCarthy, G.D., Smeed, D.A., Johns, W.E., Frajka-Williams, E., Moat, B.I., Rayner, D., Baringer, M.O., Meinen, C.S., Collins, J., Bryden, H.L., 2015. Measuring the Atlantic meridional overturning circulation at 26°N. Prog. Oceanogr. 130:91–111. http://dx.doi.org/10.1016/j.pocean.2014.10.006.
McClain, C.R., 2009. A decade of satellite ocean color observations. Annu. Rev. Mar. Sci. 1: 19–42. http://dx.doi.org/10.1146/annurev.marine.010908.163650.
Olonscheck, D., Hofmann, M., Worm, B., Schellnhuber, H.J., 2013. Decomposing the effects of ocean warming on chlorophyll a concentrations into physically and biologically driven contributions. Environ. Res. Lett. 8, 014043. http://dx.doi.org/10.1088/1748-9326/8/1/014043.
Palacz, A.P., Xue, H., Armbrecht, C., Zhang, C., Chai, F., 2011. Seasonal and inter-annual changes in the surface chlorophyll of the South China Sea. J. Geophys. Res. 116: C09015. http://dx.doi.org/10.1029/2011JC007064.
Richardson, A.J., Schoeman, D.S., 2004. Climate impact on plankton ecosystems in the Northeast Atlantic. Science 305:1609–1612. http://dx.doi.org/10.1126/science.1100958.
Rousseaux, C.S., Gregg, W.W., 2015. Recent decadal trends in global phytoplankton composition. Glob. Biogeochem. Cycles 29:1674–1688. http://dx.doi.org/10.1002/2015BG005139.
Sanchez-Franks, A., Zhang, R., 2015. Impact of the Atlantic meridional overturning circulation on the decadal variability of the Gulf Stream path and regional chlorophyll and nutrient concentrations. Geophys. Res. Lett. 42:9889–9897. http://dx.doi.org/10.1002/2015GL066262.
Schmittner, A., 2005. Decline of the marine ecosystem caused by a reduction in the Atlantic overturning circulation. Nature 434, 628–633.
Srokosz, M.A., Bryden, H.L., 2015. Observing the Atlantic meridional overturning circulation yields a decade of inevitable surprises. Science 348 (6241). http://dx.doi.org/10.1126/science.1255575.
Talley, L.D., Pickard, G.L., Emery, W.J., Swift, J.H., 2011. Descriptive Physical Oceanography: An Introduction. six edition. Published by Elserier Ltd, p. 246.
Willis, J.K., 2010. Can in situ floats and satellite altimeters detect long term changes in Atlantic Ocean overturning? Geophys. Res. Lett. 37:L06602. http://dx.doi.org/10.1029/2010GL042372.
Wu, Z., Huang, N.E., 2004. A study of the characteristics of white noise using the empirical mode decomposition method. Proc. R. Soc. Lond. A 460:1597–1611. http://dx.doi.org/10.1098/rspa.2003.1221.
Wu, Z., Huang, N.E., 2009. Ensemble empirical mode decomposition: a noise-assisted data analysis method. Adv. Adapt. Data Anal. 1:1–41. http://dx.doi.org/10.1142/S1793536909000047.
Wu, Z., Huang, N.E., Long, S.R., Peng, C.K., 2007. On the trend, detrending and variability of nonlinear and non-stationary time series. Proc. Natl. Acad. Sci. U. S. A. 104: 14889–14894. http://dx.doi.org/10.1073/pnas.0701020104.
Wu, Z., Huang, N.E., Chen, X., 2009. The multi-dimensional ensemble empirical mode decomposition method. Adv. Adapt. Data Anal. 1:339–372. http://dx.doi.org/10.1142/S1793536909000187.
Wu, Z., Huang, N.E., Wallace, J.M., Smoliak, B.V., Chen, X., 2011. On the time-varying trend in global-mean surface temperature. Clim. Dyn. 37:759–773. http://dx.doi.org/10.1007/s00382-011-1128-8.
Yoder, J.A., Kennelly, M.A., Doney, S.C., Lima, I.D., 2010. Are trends in SeaWiFS chlorophyll time-series unusual relative to historical variability? Acta Oceanol. Sin. 29:1–4. http://dx.doi.org/10.1007/s13131-010-0016-o.
Zhang, R., 2008. Coherent surface-subsurface fingerprint of the Atlantic meridional overturning circulation. Geophys. Res. Lett. 35:L20705. http://dx.doi.org/10.1029/2008GL035463.